






Article

Attenuation of the Acoustic Activity in Cement Beams under Constant Bending Load Closely Approaching the Fracture Load

Dimos Triantis ¹, Andronikos Loukidis ¹, Ilias Stavrakas ¹, Ermioni D. Pasiou ²
and Stavros K. Kourkoulis ^{2,*}

¹ Electronic Devices and Materials Laboratory, Department of Electrical & Electronic Engineering, School of Engineering, University of West Attica, 250 Thivon Av., 122 44 Athens, Greece; triantis@uniwa.gr (D.T.); a.loukidis@uniwa.gr (A.L.); ilias@uniwa.gr (I.S.)

² Laboratory for Testing and Materials, Department of Mechanics, School of Applied Mathematical & Physical Sciences, National Technical University of Athens, Zografou Campus, 157 73 Athens, Greece; epasiou@teemail.gr

* Correspondence: stakkour@central.ntua.gr; Tel.: +30-210-7721263

Abstract: The acoustic activity in beam-shaped specimens made of cement is studied, assuming that the beams are loaded in three-point bending under a step-wise loading scheme. Attention is focused to the attenuation of the acoustic activity during the constant-load stage of each specific loading step. The experimental data are analyzed in terms of the interevent time intervals between any two successive acoustic hits (using the F-function concept) and, further, in terms of the power of the acoustic hits (in terms of the recently introduced P-function). It is indicated that while the mechanical load is kept constant, the acoustic activity attenuates steadily, and during the early steps of this attenuation phase, the temporal evolution of both the F- and P-functions is excellently described by an exponential law. Moreover, it is proven that for both the F- and P-functions, the relaxation exponents decrease monotonically with increasing load. This decrease becomes quite abrupt for loads exceeding about 80% of the fracture load, providing an interesting and promising pre-failure indicator, i.e., a warning signal that the specimen is entering into the stage of impending macroscopic fracture. The specific conclusions are in very satisfactory agreement, both qualitatively and quantitatively, with similar ones drawn by considering the temporal evolution of the respective b-value.

Keywords: acoustic emissions; acoustic hits; F-function; P-function; b-value; cement-based materials; three-point bending; step-wise loading



Citation: Triantis, D.; Loukidis, A.; Stavrakas, I.; Pasiou, E.D.; Kourkoulis, S.K. Attenuation of the Acoustic Activity in Cement Beams under Constant Bending Load Closely Approaching the Fracture Load. *Foundations* **2022**, *2*, 590–606. <https://doi.org/10.3390/foundations2030040>

Academic Editors: Vladimir Frid and Stelios M. Potirakis

Received: 14 June 2022

Accepted: 19 July 2022

Published: 24 July 2022

Publisher's Note: MDPI stays neutral with regard to jurisdictional claims in published maps and institutional affiliations.



Copyright: © 2022 by the authors. Licensee MDPI, Basel, Switzerland. This article is an open access article distributed under the terms and conditions of the Creative Commons Attribution (CC BY) license (<https://creativecommons.org/licenses/by/4.0/>).

1. Introduction

In quite a few structures, a variety of structural members (beams, epistyles, plates, etc.) are loaded under various bending schemes, theoretically at a constant load level. In case such a structure is to be rehabilitated or restored, the decisions are dictated by the maximum load allowed to be applied to the members. Unfortunately, the value of this parameter is almost impossible to be determined in a member already in function, since the level of internal damage that has been accumulated within the element is unknown, and, therefore, the current values of the respective mechanical parameters are not available. To confront the problem, field measurements are necessary, permitting detection of indices that provide information about the remaining load-carrying capacity of the member. The main reason for the resultant degradation of the mechanical properties (or, equivalently, for the uncertainty about the remaining life of the element, in other words, about its remaining load-carrying capacity) is the generation and accumulation of micro-cracks.

The generation of micro-cracks in quasi-brittle and heterogeneous materials (such as, for example, cement-based products and rock-like materials), as well as their development and propagation, are quite complex natural processes. Detecting and monitoring these processes is of the utmost importance for the structural engineering community. Among

the sensing techniques used for this purpose, the use of acoustic emissions (AE) one is the most mature and well-established methods. It is widely used (both in the laboratory and for large engineering structures) to monitor crack development and to quantify the level of internal damage caused by externally applied mechanical loads, with special emphasis to the stages closely approaching that of impending macroscopic fracture [1–7].

A typical AE monitoring system records the elastic energy released (in the form of mechanical waves) during a fracture process. In fact, any displacement of lattice elements within the mass of a material is capable of generating an acoustic event, which is then recorded as an acoustic hit by a proper AE sensor. The amplitude of the acoustic hits recorded is related both to the intensity of the triggering process and to the damage mechanism responsible for the specific process [2,3]. In this context, and assuming that the temporal evolution of the acoustic signals is directly related to the generation and propagation of crack processes, the AE technique provides valuable information about the closeness of a loading scheme to the level of criticality, or equivalently, to the stage of impending macroscopic fracture [8–12].

It is well established nowadays that the AE activity in mechanically loaded brittle materials exhibits similarities with seismic activity in the earth’s crust, which is quite often described by power laws. In particular, the magnitude–frequency law, known as the Gutenberg–Richter law, is valid in the case of AE recordings in rock specimens and cement-based materials. In its most widely used formulation, the law reads as [13–15]:

$$\log_{10} N = a - b \cdot \frac{A}{20} \tag{1}$$

where A is the peak amplitude of the acoustic hits recorded (from the same sensor) expressed in decibels, N is the number of acoustic hits (the amplitude of which exceeds the respective threshold defined by the user), a is an empirical constant, and, finally, b is the AE-based b-value [13–15].

In engineering praxis, a wide variety of characteristics of the acoustic hits recorded are used in order to assess the acoustic activity and the associated level of internal damage. These characteristics can be the cumulative number of acoustic hits recorded from each sensor, the AE hits rate, the cumulative acoustic hit energy as recorded from each sensor and the corresponding rate, etc. Recently, an alternative method was proposed for the exploration of acoustic activity based on the calculation of a function, F, which is determined in terms of the inverse of the interevent time intervals, $1/\delta t_i$, of a sufficient number of consecutive acoustic hits [16,17]. Considering that the quantity of $1/\delta t_i$ represents an instant frequency (f_i) of the AE recordings, it can be said that the F-function demonstrates the variation of the mean value of n sequential f_i values. Each new value of the F-function is calculated by sliding the initial “window” by one acoustic hit. Each value of the F-function is paired to an average time instant (τ) of the time instants of the n successive hits used to calculate the specific value of the F-function. This method of representing AE activity has already been adopted by many researchers worldwide [18–26]. A significant advantage of this method for assessing acoustic activity is its capability to demonstrate the variability of the AE activity within very short time intervals. Thus, it has become a flexible tool for the description and assessment of acoustic activity during stages of the loading process with increased temporal rates of variation of the acoustic activity, as this is the stage of impending fracture where intense AE activity is recorded within an extremely short time interval.

In accordance with the F-function, valuable information about acoustic activity is provided by the temporal rate of the energy content of the acoustic hits (i.e., their power), which is quantified in terms of a function, P [27], as follows:

$$P = \frac{\sum_{i=1}^n E_i}{\Delta t} \tag{2}$$

where $\sum_{i=1}^n E_i$ is the cumulative energy of n sequential acoustic hits recorded from a single AE sensor and Δt is the duration of the time interval during which these hits were recorded. Since the AE energy is (usually) of the order of μJ , the corresponding values of the P-function are expressed in μW , while its maximum value can reach the order of pW .

In this study, the above discussed F- and P-functions are used to assess the acoustic activity in cement-mortar beams subjected to three-point bending (3PB) under a characteristic step-wise loading protocol. According to this protocol, the load increases and then it is kept constant at relatively high levels until the AE activity is practically at zero. The purpose of the study is to quantify the attenuation of the AE activity during the periods when the mechanical load is constant. It has been concluded that while decaying, the acoustic activity obeys an exponential law (the exponent of which depends on the load level). The temporal evolution of this exponent is found to be an interesting indicator warning about entrance of the specimen into its critical stage, namely, that of impending fracture, in good agreement with the respective data provided by the evolution of the b -value. The practical importance of this study lies exactly at the loading scheme considered, i.e., the gradual application of load, which is then kept constant over a long time period. The conclusions drawn provide a flexible tool, allowing engineers to estimate the level of the remaining load-carrying capacity of an element of a structure already in function. For example, it is quite common during restoration projects of stone monuments to remove damaged elements, restore/reinforce them, and then re-place them in their initial positions. If we assume that a number of elements were removed, restored, and must now be re-placed on an element, the remaining load carrying capacity of which is unknown, studying the AE attenuation could prove useful in order to decide whether or not it is safe to re-place all the restored elements. One should add one element at a time and determine the values of the exponents of the laws governing the attenuation of the acoustic activity, as their values indicate, at least approximately, whether or not fracture is impending.

2. The Experimental Protocol

Beam-shaped specimens of square cross-sections were prepared. They were made of a cement mortar mixture consisting of ordinary Portland cement, fine sand, and water at a rate of 1:3:0.5, respectively. It is noted that the size of the sand particles was between 0.6 mm and 2.0 mm, with an average size of approximately 1.1 mm, guaranteeing a relatively homogeneous structure (considering the overall size of the specimens). Wooden molds were used to host the mixture for twenty-four hours. Afterwards, the specimens were removed from the molds and cured for three months in a moisture chamber at a constant temperature (approximately 20 °C) and humidity (ranging in the interval from approximately 75% to 85%).

Three identical rigid metallic cylinders (of a diameter equal to 8 mm) were used to support and load the specimens. The load was applied at the central section of the beams (three-point bending). The stress field developed during the specific loading scheme was non-homogeneous, especially in the immediate area of the beam-loading cylinder interface. The central cross-section of the beam was under tension [28] due to the interaction of the stress field caused by bending, which was caused by the punch-effect. The specific field was maximized at the lowest side of the specimen. Therefore, taking into account that cement mortar is a brittle material (its tensile strength is much lower compared to the respective compressive one), it is reasonable to expect that fracture mechanisms are firstly activated at the lower side of the central cross-section of the specimen.

In this context, the acoustic sensor (of the R15 α type) used to detect the acoustic signals was attached on the front face of the specimens at their central cross-section (Figure 1). The PCI-2 AE acquisition system (Physical Acoustics Corp, Princeton Junction, NJ, USA) was used. The threshold for detecting acoustic events was set at 40 dB. To avoid measuring AE events coming from external sources, a frequency cutoff filter was added at the input of the acoustic sensors discarding any AE event of a frequency lower than 20 kHz.

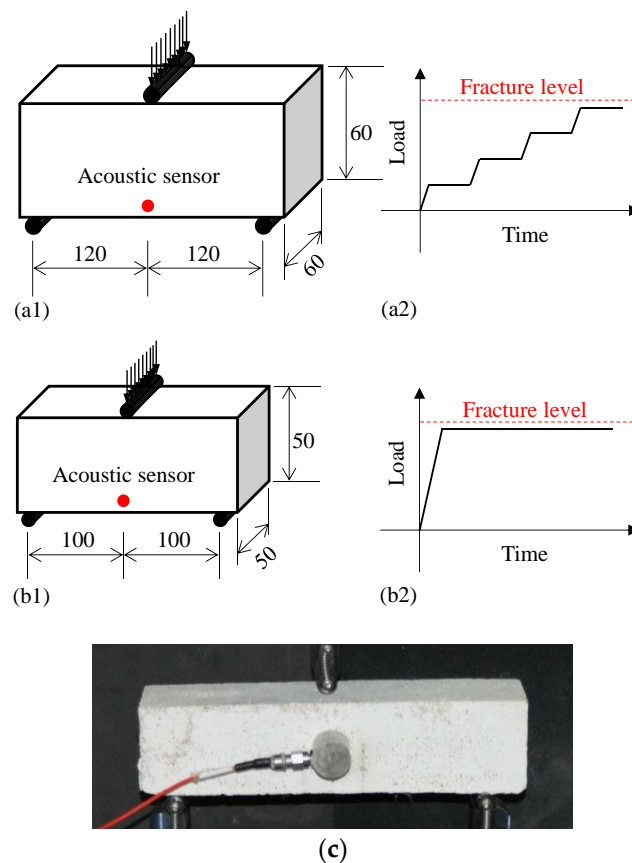


Figure 1. (a) The configuration of the beam-shaped specimens (a1,b1) (dimensions in mm), and a sketch of the loading schemes (a2,b2). (c) Photo of a typical specimen while loaded. (a2,a2) corresponds to the first protocol, while (b1–c), corresponds to the second one.

Two protocols were implemented. The first included beams dimensions of 60 mm × 60 mm × 260 mm. The supporting rollers were placed at a distance of 240 mm from each other (Figure 1a1). The fracture load for these beams was found equal to approximately 3.55 kN in terms of a preliminary series of experiments. These beams were subjected to a step-wise loading scheme: The load was increasing at a predefined level, and then it was kept constant until the complete attenuation of the acoustic activity. Then, the load was increased to a new level, and the procedure was repeated until the fracture of the specimens, which occasionally could be detected during a constant load stage, assuming that the load level attained was very close to the fracture load of the beam (Figure 1a2). A photo of a typical specimen while loaded is shown in Figure 1c.

Motivated by the interesting conclusions drawn during the first protocol regarding the very last loading stages (i.e., those very close to the fracture load), a second protocol was implemented, which focused attention to the response of the material under constant load, the level of which approaches gradually that causing fracture. In this protocol, beam dimensions of 50 mm × 50 mm × 220 mm were tested. The supporting rollers were placed at a distance of 200 mm from each other (Figure 1b1). The fracture load for these beams was found equal to 3.0 kN, again in terms of an additional preliminary series of tests. These beams were subjected to a different loading scheme: The load increased gradually, and then it was kept constant at load levels ranging from 81% to ~100% of the fracture load, with intermediate levels equal to 86%, 91%, 95%, and 98% of the fracture load.

During the experiments the quantities recorded included the load applied (by means of a calibrated load cell), the displacement of the moving traverse of the loading frame (by means of a properly calibrated Linear Variable Differential Transformer (LVDT), i.e., the

sensor used to measure very small displacements), and the acoustic hits (by means of the acoustic sensor mentioned previously).

3. Experimental Results

3.1. Multi-Step Loading Scheme

The temporal evolution of the load applied during a typical experiment of the first protocol is plotted in Figure 2a, in juxtaposition to the respective evolution of the amplitudes of the AE hits recorded. In general, the acoustic activity recorded while mechanical loading was imposed on a specimen was due to the activation of micro-damage mechanisms and micromovements of the elements of the internal structure of the tested material. The mechanical load applied and the deformation imposed, consequently, were initially responsible for generation of microcracks, which gradually coalesce, forming discontinuities at the meso- and macro-levels, leading gradually to the formation of crack networks. Each one of these natural events was accompanied by a gradually intensified release of mechanical energy, which was detected in the form of gradually intensified acoustic activity. A preloading was initially applied at a level of 2.4 kN in order to diminish parasitic AE recordings. The load was kept constant after each increase for a time interval, ensuring that the AE hit rate was reduced below the level of 1 hit per second. In this experiment, four loading steps were realized. It was seen that during the constant load stage, the acoustic activity started decaying, given that the material tended to reach a new equilibrium state, and being adapted to the geometrical and material changes imposed, while the load was increasing. During this stage, the sources of damage mechanisms were gradually eliminated and, therefore, there is no “driving force” that could maintain the acoustic activity (assuming, of course, that the material’s critical stage was not attained and that the material succeeded in reaching the new equilibrium state). Obviously, the speed towards the new equilibrium state depended on the nature of the material tested and on the current damage level, which is why the parameters of the laws describing the decay process were not constant throughout the duration of the loading protocol. The specific specimen was fractured during the fifth load-increase step, at a load of approximately 3.53 kN.

It is to be highlighted at this point that quite a few features of the AE waveforms (one could mention, for example, the time domain features such as amplitude, count, entropy, duration, energy, and frequency domain features, such as centroid frequency) are quite often used in the direction of exploring the damage mechanisms in terms of data provided by the AE technique. In this study, advantage was taken of the amplitude of the acoustic hits recorded during loading. Equally well, one could use additional features (independently or mutually combined) as described by Chai et al. [29], who considered time and frequency domain features in the direction of eliminating possible errors due to the use of limited features. As an example, the temporal evolution of the absolute energy is plotted in Figure 2b. Clearly, the conclusions drawn are qualitatively identical to those drawn from Figure 2a. It is emphasized here that during the protocol, all the necessary precautions were taken to avoid errors (as it is, for example, those due to reflected acoustic waves), including the proper calibration of the AE timing parameters (such as hit definition time, peak definition time, etc.). In this direction, preliminary tests were conducted before the onset of the main experimental procedure using schemes of strong acoustic activity. It was clearly shown that AE waves from reflections were not recorded. Obviously, in case the dimensions of the specimens or the specific characteristics of a loading protocol did not allow for proper calibration of the AE technique parameters, the option to use additional AE data was always on the table [29].

As a next step, the temporal evolution of the acoustic activity was described in terms of the F-function [16,17] (Figure 3a), and, in addition, the rate of release of the AE hit energy per unit time (power) was described in terms of the P-function [27] (Figure 3b). Again, the acoustic activity was considered in juxtaposition to the level of the externally applied load. As it is dictated by the procedure for the optimum representation of both the F- and P-functions, the time axis (τ) corresponds to the mean value of the time instants at which

the successive acoustic hits (comprising the group of hits used to calculate each value of the F- and P-functions) were recorded.

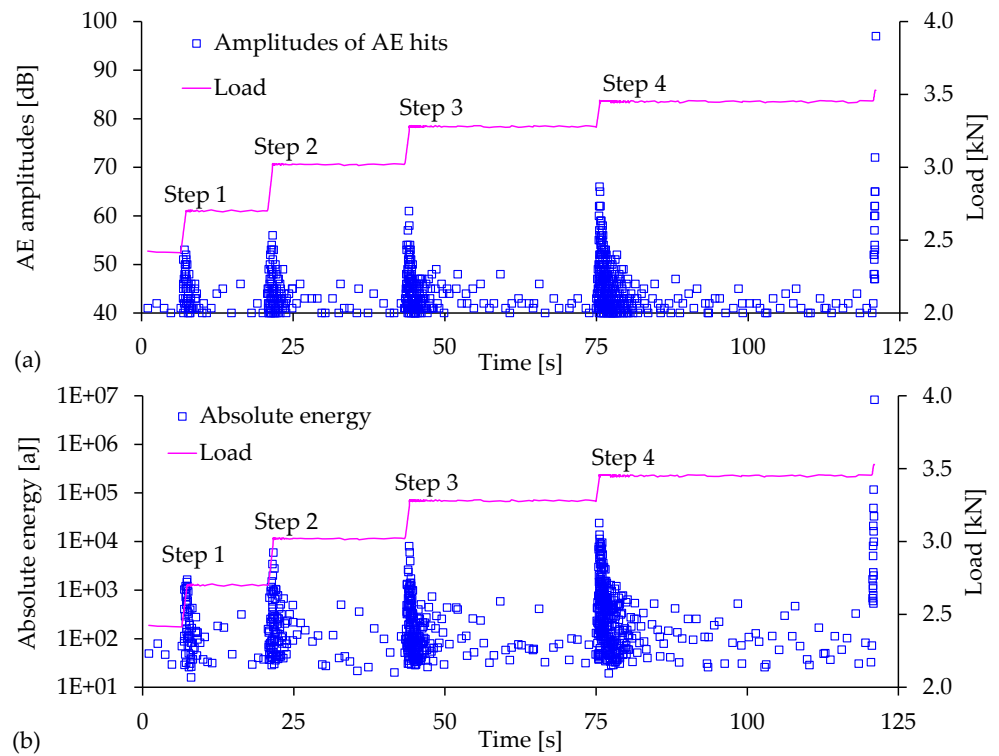


Figure 2. The temporal evolution of the load applied during a typical experiment of the first protocol, in juxtaposition to the respective evolution of the (a) amplitudes and (b) absolute energy of the AE hits recorded.

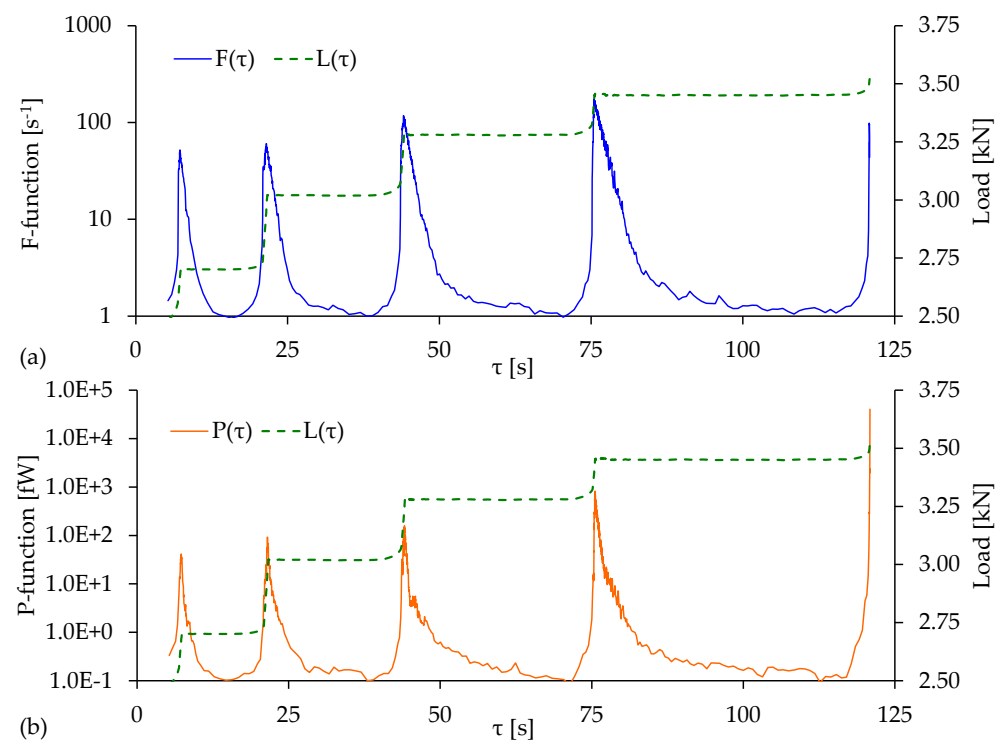


Figure 3. The temporal evolution of (a) the F- and (b) P-functions during a typical experiment of the first protocol, in juxtaposition to the respective evolution of the load applied.

In all tests of this protocol, the number of successive hits of each group used to calculate the F- and P-functions was chosen as $n = 10$. As can be seen from Figure 3a,b, while the mechanical load applied was kept practically constant, after each load increase stage, the acoustic activity decays tended to be zeroed, as was expected. This decay is discussed according to a detailed and quantitative manner in the next section.

In order now to explore the existence of a law capable of faithfully describing the relaxation (decay) of the F- and P-functions while the load applied is kept constant, both functions are plotted against the $(\tau - \tau_c)$ parameter, where τ_c is the time instant at which the load attains its maximum value at the end of the load increase phase of its loading step. Practically, this is the time instant at which both the F- and P-functions also attain their maximum values for each step of the loading scheme.

As can be clearly seen from the corresponding plots (Figure 4a–d), during the initial decay stage of the acoustic activity (i.e., for short $(\tau - \tau_c)$ intervals), both the F- and P-functions were governed by an exponential law for all four loading steps of the specific experiment. The exponential laws are of the form:

$$F = F_0 \cdot E^{-m \cdot (\tau - \tau_c)} \tag{3}$$

$$P = P_0 \cdot E^{-k \cdot (\tau - \tau_c)} \tag{4}$$

where F_0 and P_0 are numerical constants, while m and k (measured in units of inversed time, i.e., s^{-1}) are the relaxation exponents describing the intensity of the decay rate of the F- and P- functions. The inverse of both m and k is a time constant governing the exponential relaxation of the acoustic activity (in terms of either the F- or the P-function) during the time interval at which the laws of Equations (3) and (4) are valid. Low numerical values of the m and k exponents suggest a slow rate of decay of the acoustic activity, while, on the contrary, high numerical values suggest rapid relaxation. All four quantities (m , k , F_0 , and P_0) are determined by means of a proper curve fitting of the experimentally gathered data.

The coefficient of regression R^2 obtained values exceeding 0.95 for all cases, without any exception, indicating excellent simulation of the decay process by the above exponential laws. It is mentioned here that the fitting is conducted for a short time period (i.e., 1 to 2 s) after reaching the upper load level during each loading step. The least squares error fitting methodology was adopted for the AE data in this short time period. The number of the AE recordings at higher times is significantly reduced, making a reliable fitting difficult to be supported. Furthermore, provided that the data are plotted in log-linear scales, the deviation from the expected exponential decay at higher times becomes obvious.

For higher $(\tau - \tau_c)$ times, the F- and P-functions attain lower values, given that the interevent time intervals between the successive hits become longer, thus resulting in a tail of slower decay. It is quite interesting to observe that while the load level is kept constant at gradually higher levels (i.e., loads approaching the fracture level of the specimen), the m and k coefficients attain lower values.

3.2. Single-Step Loading Scheme

In order to further and convincingly support the above findings, another protocol was realized, including six additional specimens, which, for practical reasons, were of slightly smaller dimensions. As already mentioned, in this protocol, the load was applied in a single step (at a constant loading rate of 80 N/s for all six experiments of the protocol) until it attained a relatively high load level L_C , gradually approaching the fracture load. Then, it was kept constant for a time interval sufficient for the rate of the acoustic hits to decay below 1 hit/s. The results of this second protocol are plotted in Figures 5–10. The figures denoted as (a) (i.e., Figures 5a and 6a, etc.) correspond to the temporal evolution of the amplitude of the acoustic hits and that of the load applied. The figures denoted as (b) (i.e., Figures 5b and 6b, etc.) correspond to the temporal evolution of the F- and P-functions, in

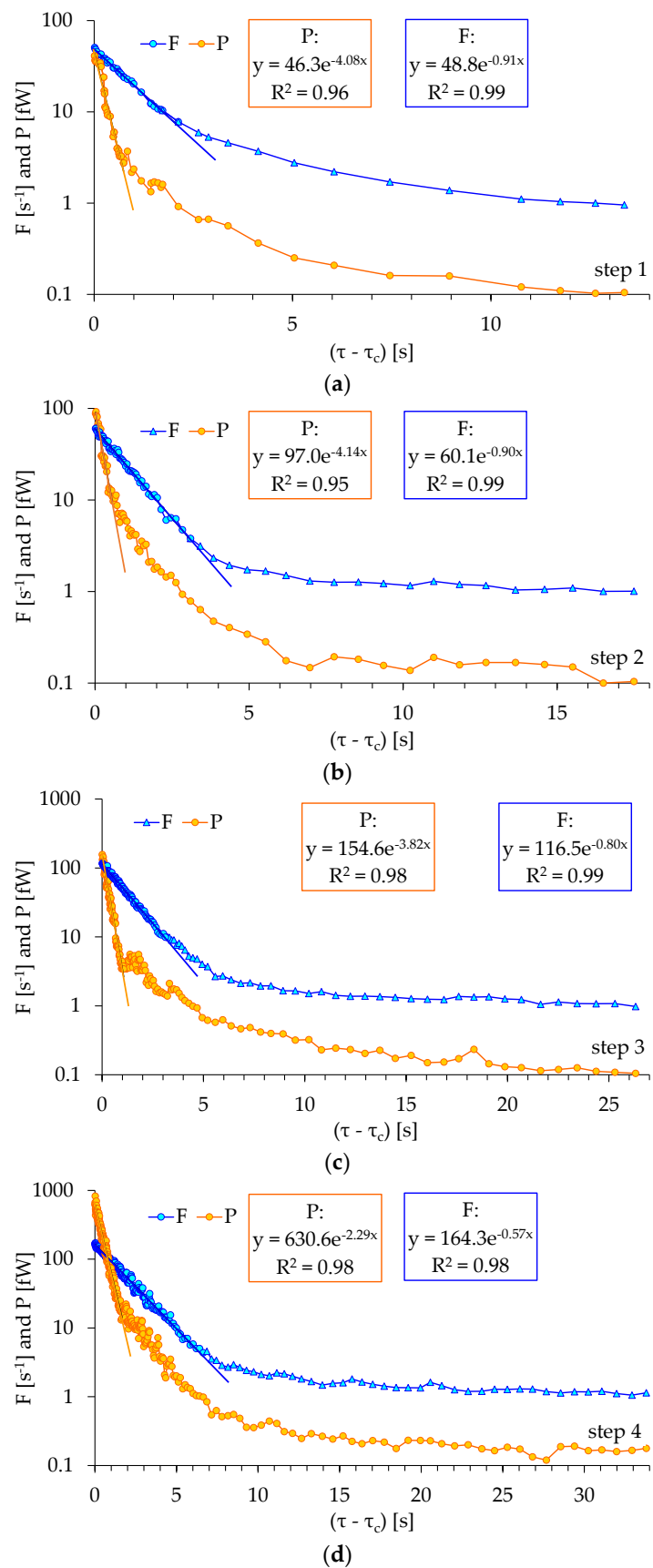


Figure 4. Decay of the AE activity in terms of the F- and P-functions (as the load applied is constant) versus the $(\tau - \tau_c)$ parameter for (a) Step 1, (b) Step 2, (c) Step 3, and (d) Step 4 of the loading protocol.

juxtaposition to the load applied. Finally, the figures denoted as (c) (i.e., Figures 5c and 6c, etc.) correspond to the evolution of the F- and P-functions in terms of the $(\tau - \tau_c)$ parameter. Each one of these figures corresponds to a specific load, i.e., Figure 5 corresponds to a normalized load, $\ell_C = 0.81$ (i.e., 81% of the fracture load), Figure 6 to $\ell_C = 0.86$, Figure 7 to $\ell_C = 0.91$, Figure 8 to $\ell_C = 0.95$, Figure 9 to $\ell_C = 0.98$, and Figure 10 to $\ell_C \approx 1.00$.

The trends detected in Figures 5–9 are qualitatively quite similar to each other. The only exception is Figure 10, which deserves special attention since the load was stabilized to $\ell_C \approx 1.00$. Indeed, during this last test, the specimen was loaded at a level equal to $L_C \approx 3.00$ kN, i.e., the fracture load of the specific specimen (and almost equal to the average fracture load obtained from the preliminary tests of this second protocol). In general, the load attained at each step is denoted as L_C , and its normalized value (over the fracture load L_f) is denoted as ℓ_C .

As can be observed in Figure 10, the specific specimen was fractured during the constant load stage, approximately 3.6 s after the load was stabilized. Indeed, as is depicted in Figure 10a (by the blue-lined arrow), approximately 2 s before macroscopic fracture, the attenuation process is interrupted and intense acoustic activity is recorded (hits of high amplitude, i.e., exceeding 55 dB, were recorded), although the load was constant. Moreover, as seen in Figure 10b, both the F- and P-functions exhibit a transient stabilization tendency, and then they start increasing rapidly, warning about the upcoming fracture of the beam [28]. During the early phase of the constant load stage, the relaxation of the acoustic activity in terms of the F- and P-functions is again described according to a quite satisfactory manner by the laws of Equations (3) and (4), respectively, at least for small values of the $(\tau - \tau_c)$ parameter (Figure 10c).

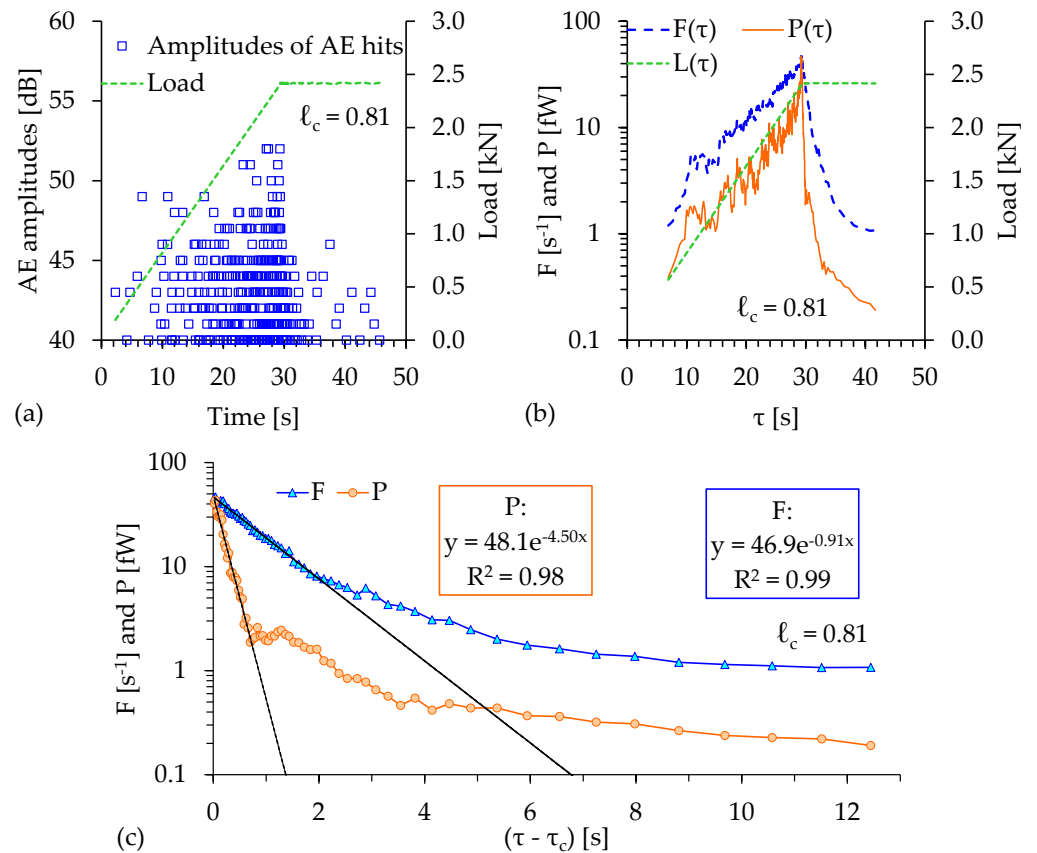


Figure 5. Temporal evolution of the amplitudes of the AE hits (a) and the F- and P-functions (b) in juxtaposition to that of the load for $\ell_C = 0.81$. (c) The decay of the acoustic activity in terms of the F- and P-functions (while the load is kept constant at $\ell_C = 0.81$) versus the $(\tau - \tau_c)$ parameter.

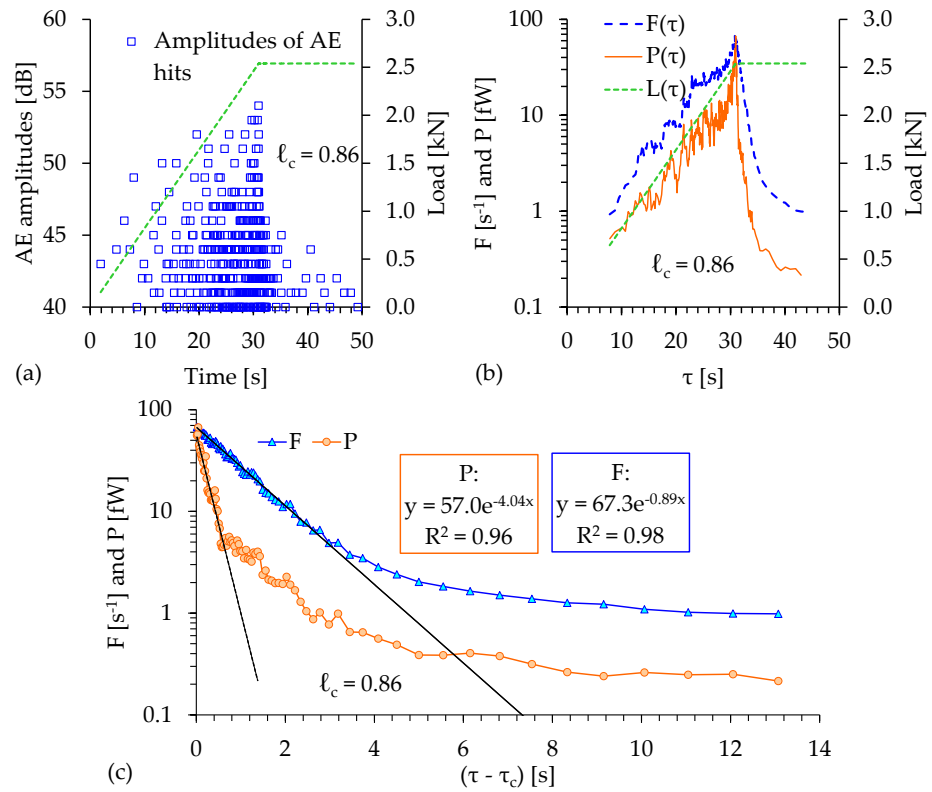


Figure 6. Temporal evolution of the amplitudes of the AE hits (a) and the F- and P-functions (b) in juxtaposition to that of the load applied for $\ell_c = 0.86$. (c) The decay of the acoustic activity in terms of the F- and P-functions (as the load is kept constant at $\ell_c = 0.86$) vs. the $(\tau - \tau_c)$ parameter.

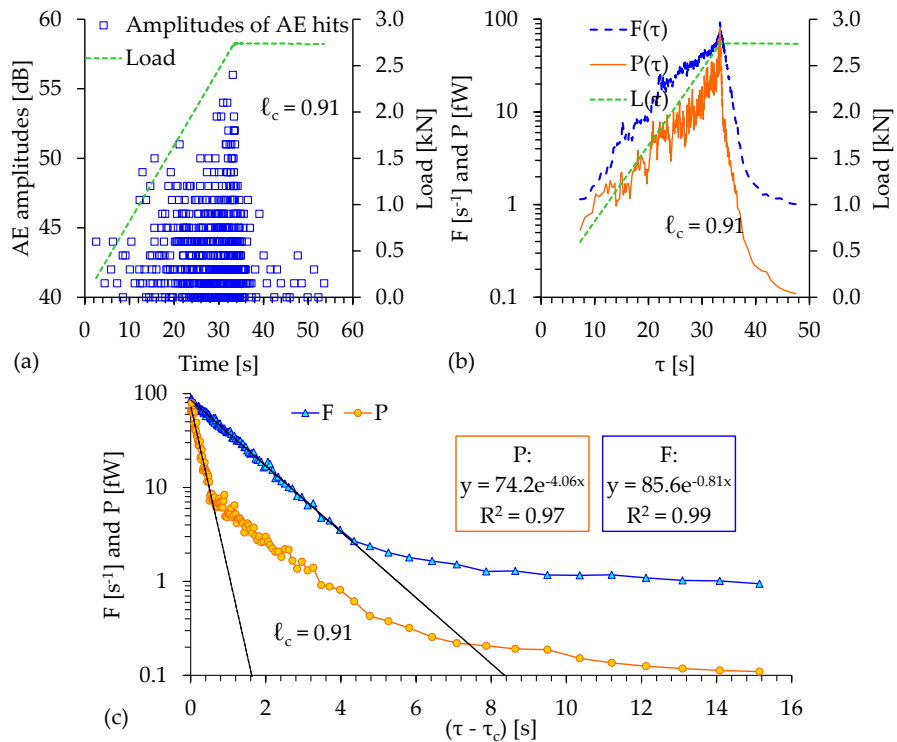


Figure 7. Temporal evolution of the amplitudes of the AE hits (a) and the F- and P-functions (b) in juxtaposition to that of the load for $\ell_c = 0.91$. (c) The decay of the acoustic activity in terms of the F- and P-functions (while the load is kept constant at $\ell_c = 0.91$) versus the $(\tau - \tau_c)$ parameter.

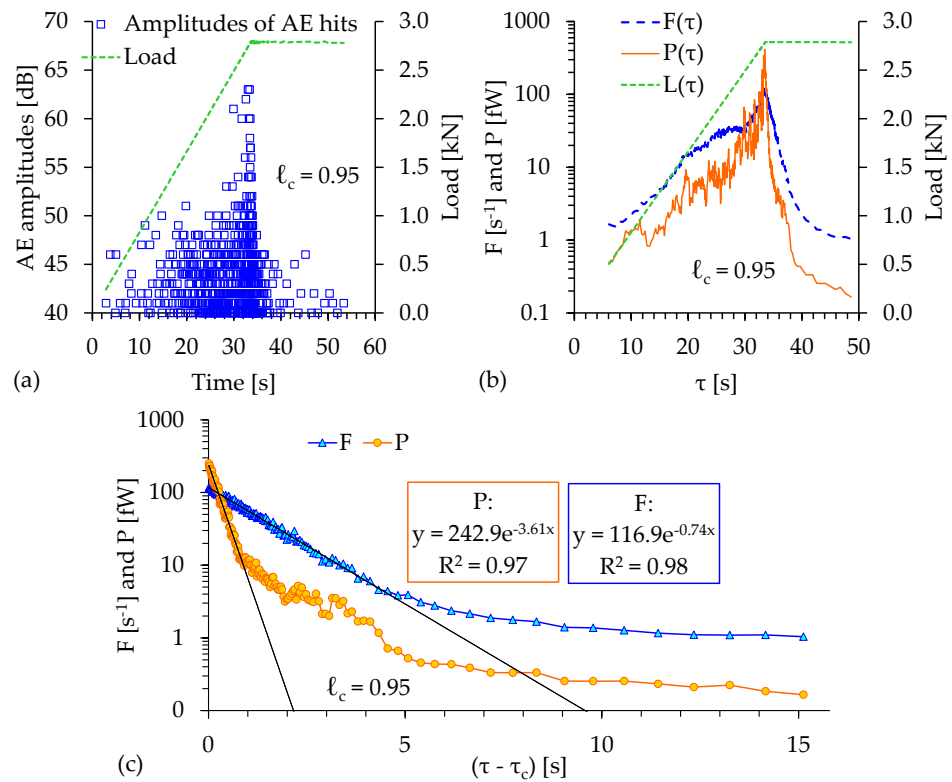


Figure 8. Temporal evolution of the amplitudes of the AE hits (a) and the F- and P-functions (b) in juxtaposition to that of the load for $\ell_C = 0.95$. (c) The decay of the acoustic activity in terms of the F- and P-functions (while the load is kept constant at $\ell_C = 0.95$) versus the $(\tau - \tau_c)$ parameter.

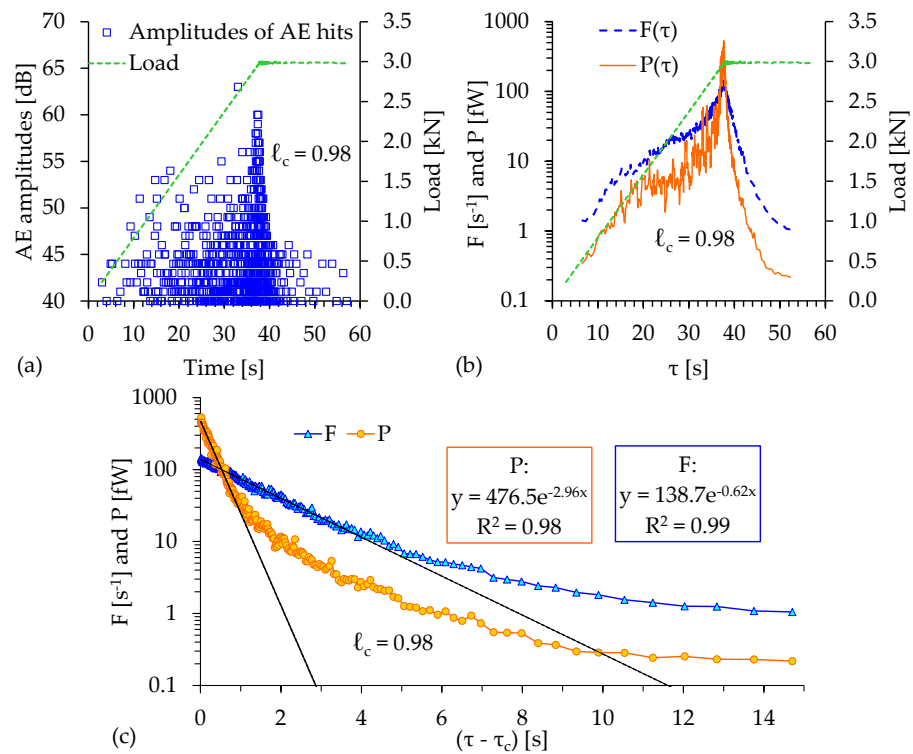


Figure 9. Temporal evolution of the amplitudes of the AE hits (a) and the F- and P-functions (b) in juxtaposition to that of the load for $\ell_C = 0.98$. (c) The decay of the acoustic activity in terms of the F- and P-functions (while the load is kept constant at $\ell_C = 0.98$) versus the $(\tau - \tau_c)$ parameter.

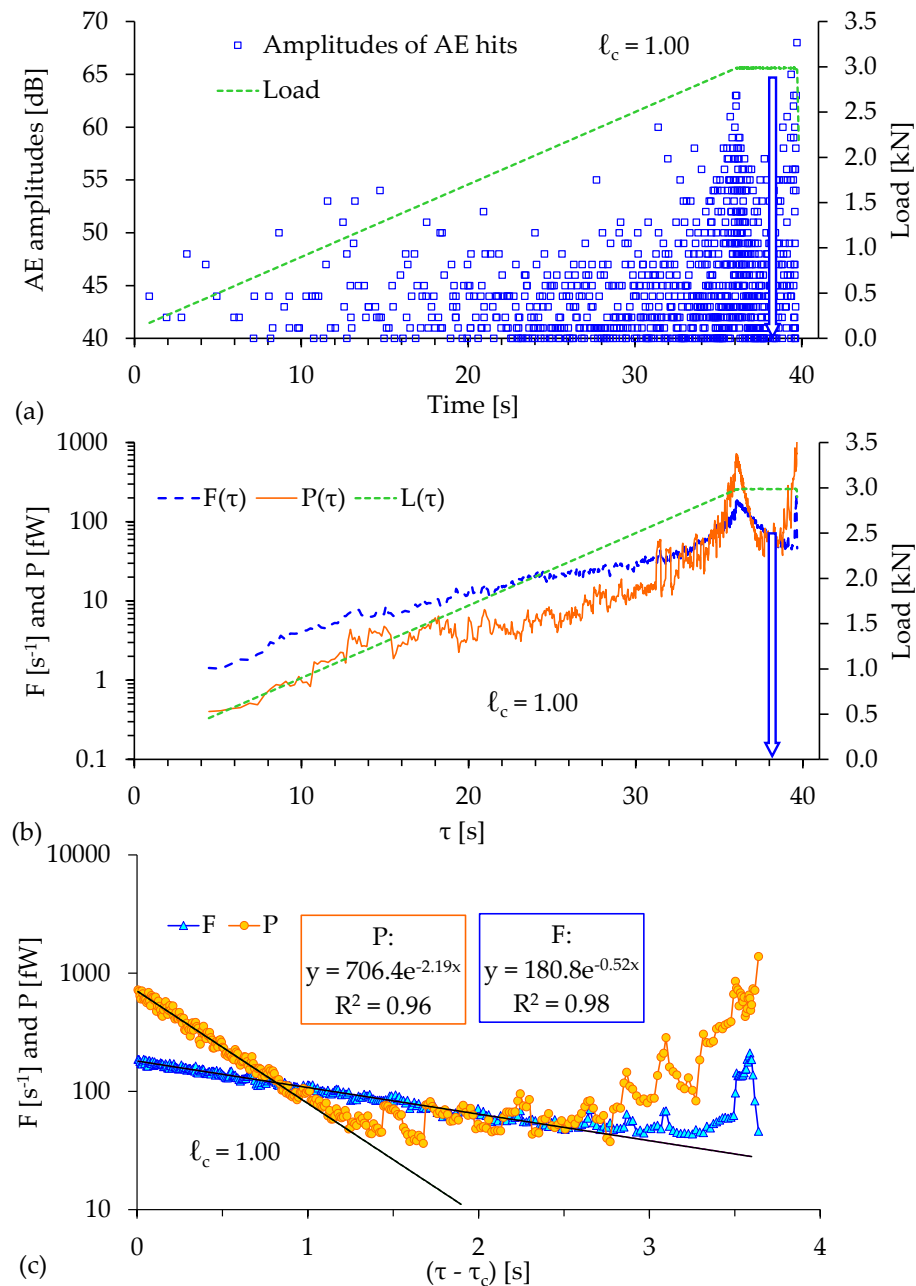


Figure 10. Temporal evolution of the amplitudes of the AE hits (a) and the F- and P-functions (b) in juxtaposition to that of the load for $\ell_c = 1.00$. (c) The decay of the acoustic activity in terms of the F- and P-functions (while the load is kept constant at $\ell_c = 1.00$) versus the $(\tau - \tau_c)$ parameter.

Comparatively, considering the strong pre-failure increases in the values of the F- and P-functions, it is seen that the increase in the P-function is more abrupt. This is attributed to the high energy acoustic hits that are recorded during this period, which result in an increased energy release of the acoustic signals, and thus to their increased power. On the other hand, these very last acoustic hits are characterized by quite a longer duration, and thus the corresponding interevent time intervals are longer, resulting in a sudden decrease in the F-function during the very last milliseconds before macroscopic fracture (Figure 10c).

4. Discussion

In Table 1, a synopsis of the experimental data presented in previous sections is exhibited, including the numerical values of the m and k exponents (quantifying the

attenuation of the acoustic hit rate and power, respectively), as well as the values of the F_o and P_o constants (see Equations (3) and (4)), which correspond (with sufficient accuracy) to the maximum values that the F- and P- functions attain (and which are recorded at the time instance τ_c), for all the experiments carried out. In addition, the fracture load, L_f , of each specimen is shown, together with the load imposed at each loading step (both its value in kN (L_c) and its normalized (over L_f) value, ℓ_c).

Table 1. Synopsis of the experimental data.

Protocol	Test	Step	L_f (kN)	L_c (kN)	ℓ_c -	F_o (s^{-1})	M (s^{-1})	P_o (fW)	K (s^{-1})
First	1	1	3.53	2.70	0.77	48.8	0.91	46.3	4.08
		2		3.02	0.86	60.1	0.90	97.0	4.14
		3		3.28	0.93	116.5	0.80	154.6	3.82
		4		3.46	0.98	164.3	0.57	630.6	2.29
Second	2	2.98	2.42	0.81	46.9	0.91	48.1	4.50	
	3	2.97	2.54	0.86	67.3	0.89	57.0	4.04	
	4	3.01	2.74	0.91	85.2	0.80	74.2	4.06	
	5	2.93	2.79	0.95	116.9	0.74	242.9	3.61	
	6	3.03	2.98	0.98	138.7	0.62	476.5	2.96	
	7	2.99	2.99	1.00	180.8	0.52	706.4	2.19	

The variation of exponents m and k and that of the constants P_o and F_o versus the load applied (normalized over the respective maximum value) are plotted in Figure 11a–d. It is very interesting to observe that the values of both decay exponents m and k exhibit a rapid decrease in load values exceeding approximately 90% of the maximum value of the load attained (see Figure 11a,b).

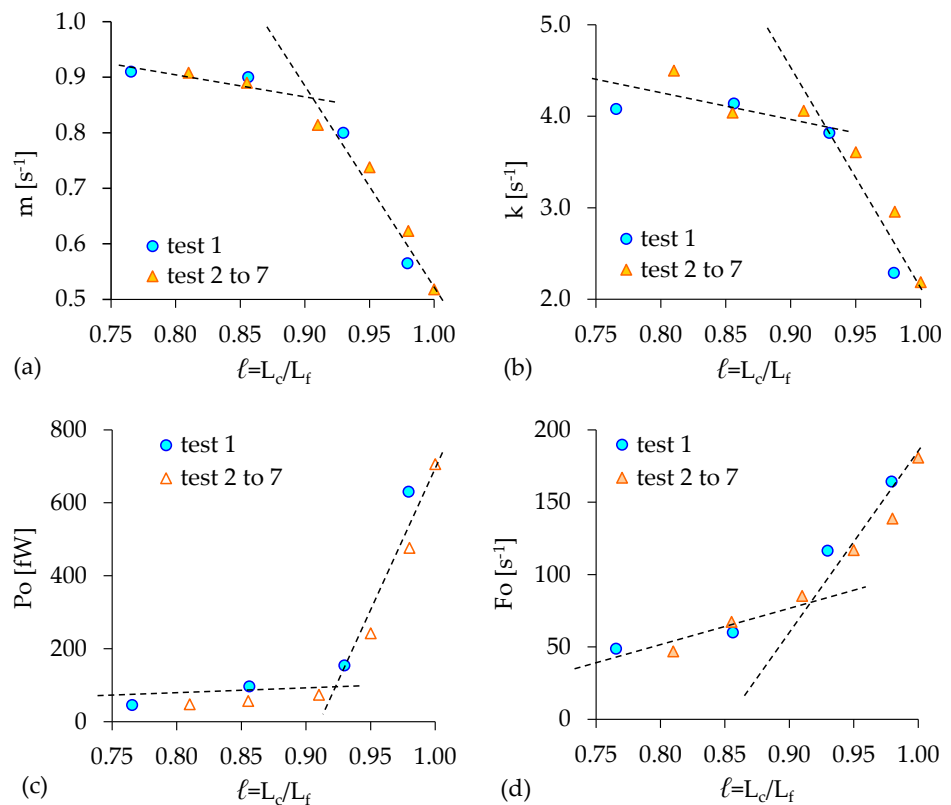


Figure 11. The variation of exponent m (a), exponent k (b), constant P_o (c), and constant F_o (d) versus the normalized (over the respective maximum value) load applied (dotted lines indicate linear fit).

A similar behavior is also observed for the pre-exponential factors F_0 and P_0 , the values of which exhibit a rapid increasing trend after the same as the above limit of $\ell_C = 0.90$ (Figure 11c,d). The above findings may be well considered as pre-failure indicators warning about the entrance of the system into its critical stage, namely, the stage of impending fracture. Quite similar conclusions have been recently drawn [30] for prismatic marble specimens loaded under step-wise compression (with a protocol similar to that adopted here). It was indicated that the acoustic activity, described in terms of the F-function, attenuates when the load imposed is kept constant. This attenuation was also found to be governed by an exponential fitting function, and the corresponding exponential factor m of Equation (3) exhibited an almost identical response to that obtained from the two protocols analyzed in the present study, although the loading scheme (three-point bending) and the specimens' materials (cement-based product) are quite different. At the same time, the acoustic hit energy release rate, expressed in terms of the P-function, also appeared to decay exponentially during the initial attenuation stage.

At this point, it is quite interesting to consider the above findings in comparison with the respective ones concerning the temporal variation of the b -value during the tests of the second protocol discussed in previous sections. In this attempt, the b -value was calculated for each test using the amplitudes of 100 sequential acoustic hits in a sliding window of 50 hits. Each b -value calculated was paired to the mean time (τ) of the 100 acoustic hits of the respective group. In order for a direct comparison to be possible, the results for all six experiments of this protocol concerning the b -value are plotted in Figure 12 versus the $(\tau - \tau_c)$ time parameter, as it was done with the quantities considered in previous section.

The overall temporal evolution of the b -values is, in general, the one expected for brittle materials. During the initial loading levels, the b -value attains relatively high levels, ranging between 2.5 and 3.2, given that the hits recorded are of a rather low amplitude. Gradually, the b -values start decreasing, and at the instant $\tau = \tau_c$, the b -value attains its minimum value. After stabilization of the load applied, i.e., for $\tau > \tau_c$, the b -value starts increasing again, systematically for all experiments, approaching high levels equal to approximately 3.5. This increase in the b -value under constant load is attributed to the decay of the amplitudes of the acoustic hits and the associated decrease in the slope of the amplitude distribution.

It is worth noticing that for experiments 5, 6, and 7, i.e., those with $\ell_C \geq 0.95$ (see the dotted ellipse in Figure 12), the b -value reaches the critical limit of $b = 1$ (it is here recalled that for these three experiments, the numerical values of the decay exponents m and k of Equations (3) and (4) exhibit considerable changes). It is well established that b -values approaching this critical limit indicate severe internal damage [31,32], thus warning that

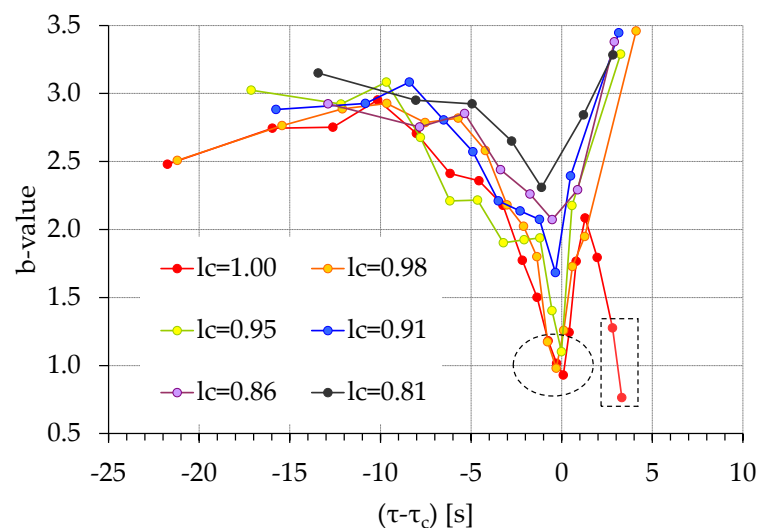


Figure 12. The temporal variation of the b -values for all six experiments of the second protocol versus the $(\tau - \tau_c)$ time parameter.

the system/specimen is about to enter into its critical stage, which is characterized by a coalescence of micro-cracks and the formation of macro-cracks. Especially in the case of experiment 7, where $l_C \approx 1.00$, and shortly after stabilization of the load, the increasing trend of the b-values is reversed and a second rapidly decreasing branch is observed, with b-values tending to the critical limit of $b = 1$ (see the dotted rectangle in Figure 12), manifesting the upcoming fracture of the specimen. It is to be noted at this point that the experimental techniques used during the protocol discussed here do not allow for direct crack observation or for a direct location of the internal cracks, and thus there is no way to provide relative direct experimental evidence. However, data related to the mechanical response of the material (as it is the axial tensile strain developed at the lower edge of the specimens, recorded with the aid of electrical strain gauges) support the statement that when b tends to 1, the strain level approaches that recorded during the fracture of specimens made of the same material [17]. In any case, the fact that as b approaches the critical value of 1, the system tends to its critical stage, is well established in the literature, especially that related to seismology [14,15] and, further, by the evidence provided by the present authors' team, who considered comparatively the b-value with other quantities providing criticality indices, as it is, for example, in the pressure stimulated currents [33].

5. Conclusions

The acoustic activity in cementitious beam-shaped specimens subjected to step-wise, three-point loading schemes was studied, paying attention to the stage during which the load is kept constant, at levels closely approaching the fracture load. The analysis of the experimentally recorded acoustic hits indicated that during this stage, the acoustic activity attenuates monotonically. Moreover, it was definitely proven that during the early period of attenuation, the temporal evolution of the acoustic activity is faithfully described by an exponential law. This law is valid independent of whether the acoustic activity is described in terms of the temporal rate of the acoustic hits (as it is here quantified by means of the F-function) or in terms of the temporal rate of the power (i.e., the time rate of the energy) of the acoustic hits (quantified here by means of the P-function). This behavior was systematically observed for all the experiments of both protocols discussed in this study.

The values of the exponential factors m and k, which somehow quantify the intensity of the attenuation of the acoustic activity, were found to strongly depend on the level of the load applied with respect to the load causing the fracture of the specimen. Both exponents were proven to exhibit a systematically decreasing tendency with an increasing load. What is more, for load levels exceeding about 90% of the fracture load, this decreasing tendency becomes quite abrupt. On the contrary, the numerical values of the pre-exponential factors F_0 and P_0 (which increase systematically with an increasing load level) exhibit a quite rapid increasing trend after the load exceeds 90% of the load that causes a macroscopic fracture of the beam.

The above-described systematic characteristics of either the m and k exponential factors or of the pre-exponential factors F_0 and P_0 could be considered as an indication that the specimen is about to enter into its critical stage, namely, that of impending macroscopic fracture or fragmentation.

The conclusions drawn, taking advantage of the temporal variation of the F- and P-functions, were found to be in excellent agreement with the respective ones obtained by considering the temporal evolution of the b-value, suggesting that this topic deserves to be further studied for a wider variety of materials and loading types.

It could be anticipated at this point that the number of tests included in this protocol (one test for the first protocol and six tests for the second protocol) is not enough, and additional data, accompanied by proper statistical analyses, are required to further support the conclusions drawn. However, it should be taken into account that the work described herein is part of an ongoing project (exploring the existence and detectability of pre-failure indices). In the frame of this protocol, the authors' team is already implementing additional

experimental protocols with different materials and various loading schemes, which will definitely support the conclusions drawn [33].

As a next step (and taking into account the importance of the issues related to the generation of cracks), it would be interesting to correlate the acoustic activity with (for example) the spatial density of the cracks within the specimen. Although this is not possible for the specific protocol (due to the fact that only one acoustic sensor was used), the authors' team has already started working on the subject, and very recently published results are extremely encouraging [27].

Author Contributions: Conceptualization, D.T. and S.K.K.; methodology, D.T., S.K.K. and I.S.; investigation, D.T., S.K.K., I.S., A.L. and E.D.P.; resources, E.D.P. and A.L.; writing—original draft preparation, S.K.K., writing—review and editing, D.T., S.K.K., I.S., A.L. and E.D.P., visualization, D.T., S.K.K., I.S., A.L. and E.D.P.; supervision, D.T. and S.K.K.; project administration, D.T. and S.K.K. All authors have read and agreed to the published version of the manuscript.

Funding: This research received no external funding.

Institutional Review Board Statement: Not applicable.

Informed Consent Statement: Not applicable.

Conflicts of Interest: The authors declare no conflict of interest.

References

- Grosse, C.; Ohtsu, M. *Acoustic Emission Testing*; Grosse, C.U., Ohtsu, M., Eds.; Springer: Berlin/Heidelberg, Germany, 2008.
- Ohtsu, M. The history and development of acoustic emission in concrete engineering. *Mag. Concr. Res.* **1996**, *48*, 321–330. [[CrossRef](#)]
- Sagar, R.V.; Prasad, B.K. A Review of recent development in parametric based acoustic emission techniques applied to concrete structures. *Nondestr. Test. Eval.* **2012**, *27*, 47–68. [[CrossRef](#)]
- Behnia, A.; Chai, H.K.; Shiotani, T. Advanced structural health monitoring of concrete structures with the aid of acoustic emission. *Constr. Build. Mater.* **2014**, *65*, 282–302. [[CrossRef](#)]
- Xu, J.; Fu, Z.; Han, Q.; Lacidogna, G.; Carpinteri, A. Micro-cracking monitoring and fracture evaluation for crumb rubber concrete based on acoustic emission techniques. *Struct. Health Monit.* **2018**, *17*, 946–958. [[CrossRef](#)]
- Kaklis, K.; Mavrigiannakis, S.; Saltas, V.; Vallianatos, F.; Agioutantis, Z. Using acoustic emissions to enhance fracture toughness calculations for CCNBD marble specimens. *Frat. Integrita Strutt.* **2017**, *11*, 1–17. [[CrossRef](#)]
- Carpinteri, A.; Lacidogna, G.; Manuello, A. The b-value analysis for the stability investigation of the ancient Athena Temple in Syracuse. *Strain* **2011**, *47*, e243–e253. [[CrossRef](#)]
- Loukidis, A.; Pasiou, E.D.; Sarlis, N.V.; Triantis, D. Fracture analysis of typical construction materials in natural time. *Phys. A* **2019**, *547*, 12381. [[CrossRef](#)]
- Loukidis, A.; Triantis, D.; Stavrakas, I.; Pasiou, E.D.; Kourkoulis, S.K. Detecting Criticality by Exploring the Acoustic Activity in Terms of the “Natural-Time” Concept. *Appl. Sci.* **2022**, *12*, 231. [[CrossRef](#)]
- Kourkoulis, S.K.; Pasiou, E.D.; Loukidis, A.; Stavrakas, I.; Triantis, D. Comparative Assessment of Criticality Indices Extracted from Acoustic and Electrical Signals Detected in Marble Specimens. *Infrastructures* **2022**, *7*, 15. [[CrossRef](#)]
- Rao, M.V.M.S.; Lakshmi, K.J.P. Analysis of b-value and improved b-value of acoustic emissions accompanying rock fracture. *Curr. Sci.* **2005**, *89*, 1577–1582.
- Carpinteri, A.; Lacidogna, G.; Pugno, N. Structural damage diagnosis and life-time assessment by acoustic emission monitoring. *Eng. Fract. Mech.* **2007**, *74*, 273–289. [[CrossRef](#)]
- Shiotani, T.; Yuyama, S.; Li, Z.W.; Ohtsu, M. Application of AE improved b-value to quantitative evaluation of fracture process in concrete materials. *J. Acoust. Emiss.* **2001**, *19*, 118–133.
- Colombo, I.S.; Main, I.G.; Forde, M.C. Assessing Damage of Reinforced Concrete Beam Using “b-value Analysis” of Acoustic Emission Signals. *J. Mater. Civ.* **2003**, *15*, 280–286. [[CrossRef](#)]
- Shearer, P.M. *Introduction to Seismology*; Cambridge University Press: Cambridge, UK, 1999; pp. 1–189.
- Triantis, D.; Kourkoulis, S.K. An Alternative Approach for Representing the Data Provided by the Acoustic Emission Technique. *Rock Mech. Rock Eng.* **2018**, *51*, 2433–2438. [[CrossRef](#)]
- Triantis, D.; Pasiou, E.D.; Stavrakas, I.; Kourkoulis, S.K. Hidden Affinities Between Electric and Acoustic Activities in Brittle Materials at Near-Fracture Load Levels. *Rock Mech. Rock Eng.* **2022**, *55*, 1325–1342. [[CrossRef](#)]
- Zhang, J.-Z.; Zhou, X.-P.; Zhou, L.-S.; Berto, F. Progressive failure of brittle rocks with non-isometric flaws: Insights from acousto-optic-mechanical (AOM) data. *Fatigue Fract. Eng. Mater. Struct.* **2019**, *42*, 1787–1802. [[CrossRef](#)]
- Niu, Y.; Zhou, X.-P.; Zhou, L.-S. Fracture damage prediction in fissured red sandstone under uniaxial compression: Acoustic emission b-value analysis. *Fatigue Fract. Eng. Mater. Struct.* **2020**, *43*, 175–190. [[CrossRef](#)]

20. Li, J.; Lian, S.; Huang, Y.; Wang, C. Study on crack classification criterion and failure evaluation index of red sandstone based on acoustic emission parameter analysis. *Sustainability* **2022**, *14*, 5143. [[CrossRef](#)]
21. Wang, X.; Wang, E.; Liu, X. Damage characterization of concrete under multi-step loading by integrated ultrasonic and acoustic emission techniques. *Constr. Build. Mater.* **2019**, *221*, 678–690. [[CrossRef](#)]
22. Yao, W.; Yu, J.; Liu, X.; Zhou, X.; Cai, Y.; Zhu, Y.L. Study on acoustic emission characteristics and failure prediction of post-high-temperature granite. *J. Test. Eval.* **2019**, *48*, 2459–2473.
23. Ge, Z.; Sun, Q. Acoustic emission characteristics of gabbro after microwave heating. *Rock Mech. Rock Eng.* **2021**, *138*, 104616.
24. Saltas, V.; Peraki, D.; Vallianatos, F. The use of acoustic emissions technique in the monitoring of fracturing in concrete using soundless chemical demolition agent. *Frat. Integrita Strutt.* **2019**, *13*, 505–516. [[CrossRef](#)]
25. Zhou, X.; Niu, Y.; Cheng, H.; Berto, F. Cracking behaviors and chaotic characteristics of sandstone with unfilled and filled dentate flaw. *Theor. Appl. Fract. Mech.* **2021**, *112*, 102876. [[CrossRef](#)]
26. Huang, J.; Liao, Z.; Hu, Q.; Song, Z.; Wang, X. Fracture mechanism of tight sandstone under high and complex 3-D stress compression: Insights from acoustic emission. *J. Pet. Sci. Eng.* **2022**, *208*, 109635. [[CrossRef](#)]
27. Triantis, D.; Stavrakas, I.; Loukidis, A.; Pasiou, E.D.; Kourkoulis, S.K. Exploring the acoustic activity in brittle materials in terms of the position of the acoustic sources and the power of the acoustic signals—Part I: Founding the approach. *Forces Mech.* **2022**, *7*, 100088. [[CrossRef](#)]
28. Stergiopoulos, C.; Stavrakas, I.; Triantis, D.; Vallianatos, F.; Stonham, J. Predicting fracture of mortar beams under three-point bending using non-extensive statistical modeling of electric emissions. *Phys. A* **2015**, *419*, 603–611. [[CrossRef](#)]
29. Chai, M.; Hou, X.; Zhang, Z.; Duan, Q. Identification and prediction of fatigue crack growth under different stress ratios using acoustic emission data. *Int. J. Fatigue* **2022**, *160*, 106860. [[CrossRef](#)]
30. Triantis, D.; Stavrakas, I.; Pasiou, E.D.; Kourkoulis, S.K. Assessing the acoustic activity in marble specimens under stepwise compressive loading. *Mat. Design Process. Comm.* **2020**, *2*, e100. [[CrossRef](#)]
31. Shiotani, T.; Ohtsu, M.; Ikeda, K. Detection and evaluation of AE waves due to rock deformation. *Constr. Build. Mater.* **2001**, *15*, 235–246. [[CrossRef](#)]
32. Aggelis, D.G.; Soulioti, D.V.; Sapouridis, N.; Barkoula, N.M.; Paipetis, A.S.; Matikas, T.E. Acoustic emission characterization of the fracture process in fiber reinforced concrete. *Constr. Build. Mater.* **2011**, *25*, 4126–4131. [[CrossRef](#)]
33. Stavrakas, I.; Kourkoulis, S.; Triantis, D. Damage evolution in marble under uniaxial compression monitored by Pressure Stimulated Currents and Acoustic Emissions. *Frat. Integrita Strutt.* **2019**, *13*, 573–583. [[CrossRef](#)]